Available online at https://link.springer.com/journal/42241
http://www.jhydrodynamics.com
**Journal of Hydrodynamics**, 2025
https://doi.org/10.1007/s42241-025-0065-7

# Space-time correlations of near-wall velocity and pressure fluctuations in wall-resolved and wall-modeled large-eddy simulation

Guo-qing Fan[1], Han-qiao Han[2], Wei-wen Zhao[1], De-cheng Wan[1*]
1. *Computational Marine Hydrodynamics Lab (CMHL), School of Ocean and Civil Engineering, Shanghai Jiao Tong University, Shanghai 200240, China*
2. *Wuhan Second Ship Design and Research Institute, Wuhan 430205, China*

(Received July 23, 2025, Revised August 16, 2025, Accepted August 17, 2025, Published online November 27, 2025)


**Abstract:** Wall-resolved large-eddy simulation (WRLES) and wall-modeled large-eddy simulation (WMLES) of turbulent channel flow at $Re_\tau \approx 1\,000$ are performed to explore their capabilities in predicting the space-time correlations of near-wall velocity and pressure fluctuations. Our findings indicate that both WRLES and WMLES can effectively capture the essential features in the wavenumber-frequency spectra. Doppler shifts due to the convection velocity and Doppler broadening caused by the random sweeping effects of large-scale eddies are observed in the wavenumber-frequency spectra. Both methods predict the near-wall velocity fluctuations with reasonable accuracy, but predicting wall pressure fluctuations seems to be more challenging for the current wall modeling approach. Without resolving the viscous sublayer, WMLES slightly overestimates the spectral levels of wall pressure fluctuations in low-wavenumber (or frequency) region. In addition, the two-dimensional spatial spectra indicate that isotropic subgrid-scale models may struggle to accurately capture the anisotropy of small-scale eddies near the wall.

**Key words:** Space-time correlation, wavenumber-frequency spectra, wall-modeled large-eddy simulation, wall pressure fluctuation

## 0. Introduction

As an unresolved challenge in classical mechanics, the complexity of wall-bounded turbulence stems from its highly chaotic and nonlinear nature. In many fields such as aerospace and ocean engineering, the study of near-wall velocity is crucial for turbulence control and optimizing engineering designs. Meanwhile, wall pressure fluctuations are considered as the primary source of noise generated by turbulent wall-bounded flows. The study of wall pressure fluctuations is vital for unveiling the fundamental nature of flow-induced noise and refining turbulence models.

Over the past few decades, numerous scholars have conducted experimental researches on near-wall velocity and wall pressure fluctuations. The research scope has evolved from simple root mean square of pressure fluctuations and one-dimensional spectra to encompass wavenumber-frequency spectra capable of reflecting the space-time correlations of turbulence. Based on experimental observations, many theoretical models have been proposed to describe the space-time correlations of near-wall turbulence. Regarding velocity fluctuations, milestone studies include the Taylor frozen-flow hypothesis[1] and the random sweeping model[2-3]. Taylor suggested that vortices of different scales in a flow move downstream at a constant velocity with minimal distortion, leading to the concentration of all energy in the convective ridge of the wavenumber-frequency spectra. However, this model has significant limitations in near-wall flow and free shear flow. Kraichnan[2] and Tennekes[3] proposed the random sweeping model, which incorporates a sweeping velocity to account for vortex distortion.

Due to the limitations of size and sensitivity of practical sensors, experimental measurements often struggle to accurately capture all the details within the flow field. In recent years, with the rapid advancement of computers, numerical simulation is becoming an important tool for analyzing space-time correlations in turbulence. Direct numerical simulation (DNS), as a highly accurate simulation approach, directly solves the Navier-Stokes equations on a very fine grid and

Project supported by the National Natural Science Foundation of China (Grant No. 52131102).
**Biography:** Guo-qing Fan (2000-), Male, Ph. D. Candidate,
E-mail: fanguoqing@sjtu.edu.cn.
**Corresponding author:** De-cheng Wan,
E-mail: dcwan@sjtu.edu.cn

captures almost every detail in the unsteady flow fields. Over the past few decades, many scholars have conducted DNS of turbulent channel flow at various Reynolds numbers to study the underlying mechanisms of wall pressure fluctuations. Lee and Moser[4] conducted DNS of turbulent channel flow up to $Re_\tau = 5\,200$, with a particular focus on the wall-bounded flow at high Reynolds number. A distinct separation of scales between inner-layer and outer-layer structures at high Reynolds numbers was observed in the pre-multiplied energy spectra of velocity fluctuation. The DNS database established by Lee and Moser[4] were further analyzed by Panton et al.[5] to study the near-wall pressure fluctuations. For wall-bounded flow at high Reynolds number, the phenomenon of inner-outer scale separation was also observed in the pre-multiplied spectra of pressure fluctuations and the outer-layer contribution to wall pressure becomes more important. Yang and Yang[6] performed DNS of channel flow at $Re_\tau = 1\,000$ and compared the wavenumber-frequency spectra of wall pressure fluctuations and the streamwise velocity fluctuations at $y^+ \approx 15$. They pointed out that the wavenumber-frequency spectra of wall pressure fluctuations have a similar functional form to that of velocity fluctuations.

Apart from the DNS studies above, large-eddy simulation (LES) has also gained significant attention in studying turbulence characteristics and replacing Reynolds-averaged Navier-Stokes (RANS) simulations in many fields. He et al.[7] compared different subgrid-scale (SGS) models of LES for predicting space-time correlations of velocity fluctuations. Wilczek et al.[8] investigated the wavenumber-frequency spectra of streamwise velocity fluctuations through LES. The wavenumber-frequency spectra provided a clear observation of the Doppler shift and Doppler broadening phenomena. However, in high Reynolds number flows, the majority of the mesh is needed to resolve the inner layer of the boundary layer. The computational costs of wall-resolved large-eddy simulation (WRLES) are still prohibitive.

To save computational costs near the wall, wall-modeled large-eddy simulation (WMLES) has gained attention and many wall modeling methods[9-11] have been proposed over the past several decades. They can be mainly divided into two categories: One is the hybrid LES/RANS method, where the LES equations are solved only above the “interface” and the near-wall region is typically treated using RANS method. Another category is the wall stress model, which introduces wall stress boundary conditions to replace the no-slip boundary condition, providing correct wall stress boundary conditions on a coarse near-wall grid. This paper mainly focuses on the latter and recently it has been successfully applied to various flows such as turbulent channel flows[12-15], separated flows[16-18], and high Reynolds number flows[19-20], effectively addressing the log-layer mismatch (LLM) issue observed in the near-wall velocity profiles with coarse mesh resolutions. However, previous studies[12, 21-25] on WMLES have largely focused on mean flow quantities. Although some scholars have begun to shift their focus towards the predictive capabilities of WMLES for flow fluctuations[26] and near-wall turbulent coherent structures[27], systematic studies on the space-time correlations of near-wall velocity and pressure fluctuations in WMLES are still limited. This is particularly significant because, compared with RANS, our expectations for LES lie more in predicting fluctuation quantities and even utilizing it to study the flow mechanics of turbulence. Moreover, compared with velocity fluctuations, there has been relatively less research on the space-time correlations of wall pressure fluctuations, which is a crucial issue that needs to be addressed for the studies of flow-induced noise.

In present study, turbulent channel flow at $Re_\tau \approx 1\,000$ is numerically simulated using both WRLES and WMLES methods to investigate their capabilities in predicting the space-time correlations of near-wall velocity and pressure fluctuations. Various spectra analysis techniques are employed in this study to provide a more comprehensive understanding of the WMLES. The results are compared with DNS data[6].

## 1. Numerical methodology

### 1.1 *Governing equations*

LES is incapable of resolving vortices of all scales in the flow field. By applying a filter to the incompressible Navier-Stokes equations, the governing equations for LES can be obtained.

$$\frac{\partial \tilde{u}_i}{\partial t} + \frac{\partial \tilde{u}_i \tilde{u}_j}{\partial x_j} = -\frac{1}{\rho}\frac{\partial \tilde{p}}{\partial x_i} + \nu \frac{\partial^2 \tilde{u}_i}{\partial x_j \partial x_j} - \frac{\partial \tau_{ij}^{\mathrm{SGS}}}{\partial x_j} \tag{1}$$

$$\frac{\partial \tilde{u}_i}{\partial x_i} = 0 \tag{2}$$

where $\tilde{u}_i\,(i = 1,2,3)$ is the filtered velocity component in the $x_i$ direction, $\tilde{p}$ is the filtered pressure, $\nu$ is the kinematic viscosity of the fluid and $\tau_{ij}^{\mathrm{SGS}}$ is the SGS stress term which is given by:

$$\tau_{ij}^{\mathrm{SGS}} = 2\nu_{\mathrm{SGS}}\tilde{S}_{ij} + \frac{1}{3}\tau_{kk}^{\mathrm{SGS}}\delta_{ij} \tag{3}$$

where $\tilde{S}_{ij}$ is the resolved strain-rate tensor, $\delta_{ij}$ is the Kronecker delta, $\nu_{\mathrm{SGS}}$ is the SGS eddy viscosity. In this study, the wall-adapting local eddy-viscosity (WALE) model[28] is applied to compute the eddy viscosity.

$$\nu_{\mathrm{SGS}} = (C_{\mathrm{w}}\Delta)^2 \frac{(S_{ij}^d S_{ij}^d)^{3/2}}{(\tilde{S}_{ij}\tilde{S}_{ij})^{5/2} + (S_{ij}^d S_{ij}^d)^{5/4}} \tag{4}$$

where $C_{\mathrm{w}} = 0.325$ is the WALE coefficient, $\Delta$ is the cube root of local cell volume, $S_{ij}^d$ is the traceless symmetric part of the square of the velocity gradient tensor.

1.2 *Near-wall modeling*

For WMLES, the filtered Navier-Stokes equation is solved on relatively coarse near-wall grids. The coarse grids struggle to accurately predict the sharp velocity gradients near the wall, often leading to the LLM phenomenon. The wall stress model addresses this by applying a wall stress boundary condition instead of the no-slip boundary condition. Specifically, the wall stress model corrects the boundary condition of the turbulent viscosity, thus obtaining the correct wall shear stress on coarse grids near the wall. This approach is based on the simplified thin boundary layer equations (TBLE)[29]. In the inner layer of the boundary layer, the pressure gradient in the wall-normal direction is assumed to be zero and the filtered N-S equations within the boundary layer can be simplified as the TBLE:

$$\frac{\partial}{\partial x_2}\left[(\nu + \nu_t)\frac{\partial \tilde{u}_i}{\partial x_2}\right] = F\ , \quad i = 1, 3, \cdots \tag{5}$$

where $F_i$ is source term, including pressure gradient terms, transient terms, and convection terms. The turbulent eddy viscosity is obtained from the mixing length theory with a near-wall damping function

$$\nu_t = \kappa \nu x_2^+ (1 - \mathrm{e}^{-x_2^+/A})^2 \tag{6}$$

where $A = 17.8$. Given that the focus of this study is turbulent channel flow, where the flow state is approximately in equilibrium, the equilibrium wall stress model (EQWM)[30] is used in the present study and the source term $F_i$ in Eq. (5) is set to zero. By integrating Eq. (5) from the wall to the sampling point, the boundary condition for wall shear stress can be obtained.

## 2. Numerical settings

2.1 *Computational domain and mesh*

The computational domain and mesh are described below. Figure 1 shows the computational domain which is used for all the simulations in present study. The domain is set up following the same configuration as the DNS computations of Yang and Yang[6]. Specifically, the domain size is set to $L_x \times L_y \times L_z = 4\pi\delta \times 2\delta \times 2\pi\delta$, where $\delta$ is the channel half-height, $x$, $y$ and $z$ denote the streamwise, wall-normal and spanwise directions. As for the boundary conditions, periodic boundary conditions are applied in the streamwise and spanwise directions, while a no-slip velocity boundary condition and a zero-gradient pressure condition are applied for both the top and bottom walls. A source term is introduced into the momentum equation to maintain the bulk mean velocity $U_{\mathrm{b}}$ to a constant, which ensures the Reynolds numbers based on the bulk velocity and friction velocity equal to $Re_{\mathrm{b}} = U_{\mathrm{b}}\delta/\nu = 20\,000$, $Re_\tau = u_\tau \delta/\nu = 1\,000$, where $u_\tau = \sqrt{\tau_{\mathrm{w}}/\rho}$ is the wall friction velocity.

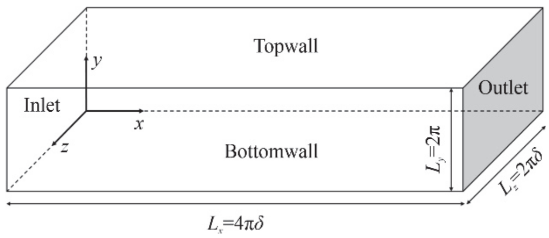


Fig. 1 Computational domain

The key parameters of meshes are demonstrated in Table 1, where $N_x \times N_y \times N_z$ are the numbers of grid points in three directions, $\Delta x^+$, $\Delta y^+$ and $\Delta z^+$ are the non-dimensional grid spacings. In this paper, variables with superscript "+" denote non-dimensionalized using characteristic length $\nu/u_\tau$ and characteristic velocity $u_\tau$. As WMLES only models the inner layer of the boundary layer, we strive to ensure the mesh resolution consistency between WRLES and WMLES in the outer layer of the boundary layer as much as possible. In terms of sampling height, some studies[10, 31] have suggested that setting the sampling height at the first cell off the wall may lead to LLM. In present study, the sampling height is set at the fourth cell center, $h = 4^{\mathrm{th}}$ and the distance of the sampling point from the wall is $\Delta h_{\mathrm{wm}}^+ = 36.4$.

**Table 1 Parameters of computational meshes**

| Case | $N_x \times N_y \times N_z$ | $\Delta x^+$ | $\Delta y^+$ | $\Delta z^+$ |
|---|---|---|---|---|
| WRLES | 629×217×629 | 20.00 | 0.79-15.00 | 10.00 |
| WMLES | 629×141×629 | 20.00 | 10.00-15.00 | 10.00 |

2.2 *Numerical schemes and solvers*

In terms of the numerical schemes and solvers, the coupled pressure-velocity is solved using the PISO algorithm. The temporal term employs the second-order implicit backward scheme. The gradient and Laplacian terms are discretized using the second-order linear scheme. Regarding the discretization of the convective term, WRLES and WMLES employ different numerical discretization schemes. For WRLES, the second-order central differencing is used for the convection term in the N-S equations. However, for WMLES, given the relatively coarse grid near the wall, employing the linear interpolation scheme used in WRLES could potentially introduce numerical oscillations. The use of the linear upwind scheme will introduce additional numerical dissipation, but it provides relatively better computational stability. In present study, numerical simulation for WMLES adopt the linear upwind stabilized transport (LUST) scheme[32-33]. This scheme uses a weighted average of 75% linear central and 25% linear upwind scheme to compute cell-face values, resulting in second-order accuracy.

## 3. Results and discussion

In this section, we conduct numerical simulations of channel flow at $Re_\tau \approx 1\,000$ employing both WRLES and WMLES methods. Simulations are run for 20 flow-past times, with the first 10 flow-past times used for flow development and the remaining 10 flow-past times used for statistical analysis. Although WMLES resolves the buffer layer with approximately 64.8% of the grid required by WRLES, solving the viscous sublayer often necessitates more pressure iterations. The actual computational cost, measured in core-hours, is only 20% of that for WRLES, indicating a significant improvement in computational efficiency for WMLES. In the subsequent studies, we first perform a visualization analysis of the vortex structures. Subsequently, we compare the predictive accuracy of both methods in terms of mean quantities. Finally, the predictive accuracy of both methods for space-time correlations of near-wall velocity and pressure fluctuations are studied with the help of various spectral analysis.

3.1 *Instantaneous flow field*

Figure 2 shows the instantaneous near-wall vortical structures visualized by the $Q$-criterion. The vortical structures are colored by instantaneous streamwise velocity normalized by the bulk mean velocity $U_b$. Due to the approximate symmetry of the channel flow, only the vortex structures from the bottom wall to the center of the channel are presented here. As the distance from the wall increases, the size of the vortices also increases. The multi-scale phenomena of wall-bounded turbulent flow is well observed. Compared with WMLES, WRLES appears to capture the near-wall vortex structures with greater detail.

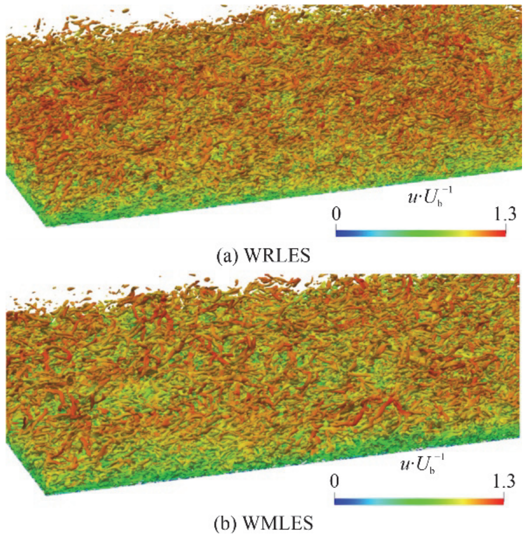


Fig. 2 Instantaneous near-wall vortical structures visualized by the $Q$-criterion $(Q = 0.05)$

Figure 3 displays the space-time contours of streamwise velocity fluctuations at $y^+ = 15$. The horizontal axis represents the spatial distribution of probes, while the vertical axis denotes time across the computational domain. From Figs. 3(a), 3(c), the convection characteristics and the random sweeping effects can be clearly observed. However, in Figs. 3(b), 3(d), only the random sweeping of large-scale vortices over small-scale vortices and the distortions caused by the interactions of small-scale vortices can be observed. The streamwise and spanwise directions exhibit different space-time distribution patterns.

3.2 *Mean velocity profile and Reynolds stress*

Figure 4 shows the mean streamwise velocity profile. The wall friction velocities $u_\tau$ obtained by WRLES and WMLES are $9.93\times10^{-3}$, $1.02\times10^{-2}$. Compared with the DNS[6] value of $9.98\times10^{-3}$, the prediction errors of WRLES and WMLES are –0.5%, 2.3%. The results of WRLES match well with DNS data in both the viscous sublayer and logarithmic layer. The current wall model slightly overestimates the wall friction velocity, leading to a velocity profile in the logarithmic layer that is slightly lower than the DNS results.

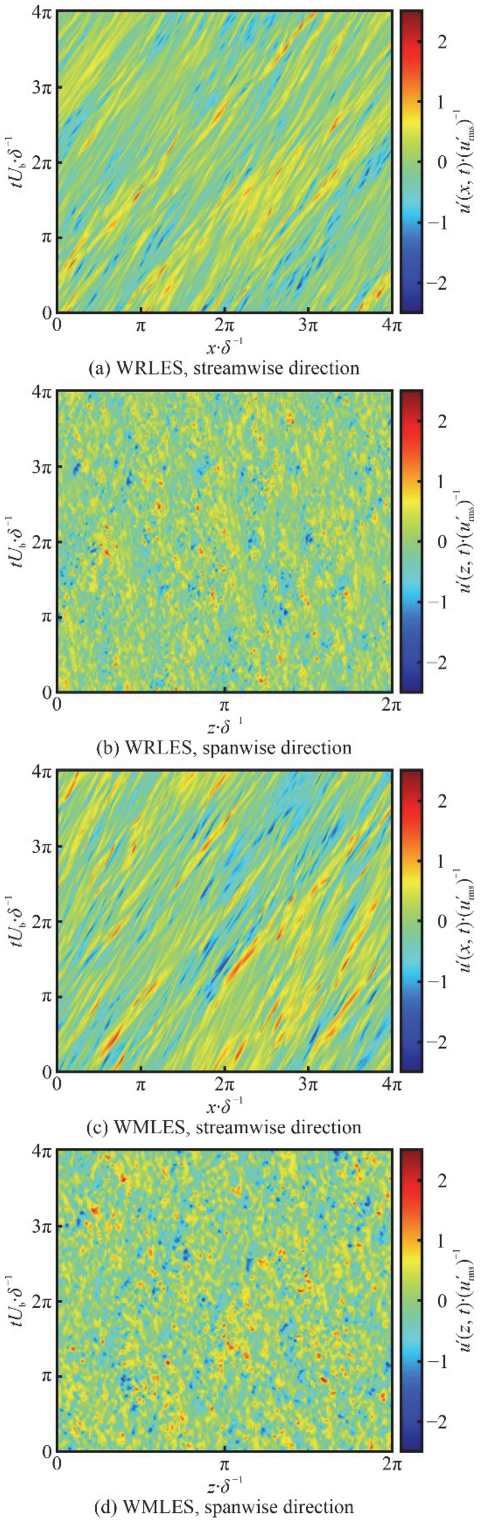


Fig. 3 Space-time contours of streamwise velocity fluctuations at $y^+ = 15$ along different direction

Figure 5 shows the resolved Reynolds stresses in inner scaling, which are compared with the DNS data[6]. The red line represents the results of WRLES, the blue line represents the results of WMLES, and the black line shows the DNS results. For the Reynolds stress components $\langle v'v' \rangle^+$, $\langle w'w' \rangle^+$ and $\langle u'v' \rangle^+$, the agreement between the DNS data and the two methods is satisfactory. For the $\langle u'u' \rangle^+$ component, the result of WRLES matches well with DNS data in the inner layer but show relatively underprediction in the outer layer. In the case of WMLES, despite the relatively coarse near-wall grid, the Reynolds stress $\langle u'u' \rangle^+$ at corresponding grid points compares favorably with the DNS results, with differences being acceptable. The peak of $\langle u'u' \rangle^+$ predicted by WMLES is 7% higher compared with the DNS results. Overall, in terms of mean flow quantities, both WRLES and WMLES agree well with DNS.

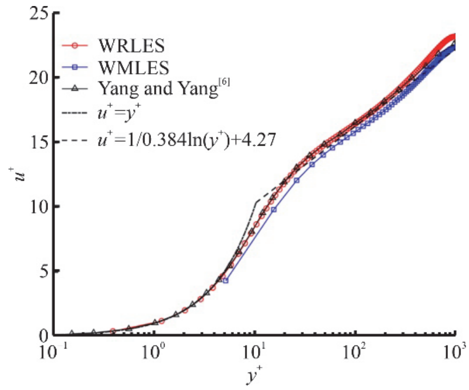


Fig. 4 Mean streamwise velocity profiles

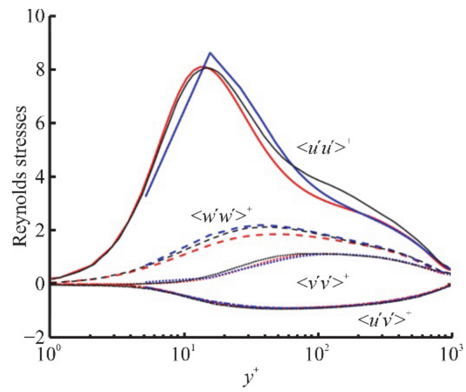

Fig. 5 Inner-scaled Reynolds stresses

### 3.3 *One-dimensional spectra*

In the following section, we further investigate the performance of WRLES and WMLES in predicting fluctuation quantities and the space-time correlations of near-wall turbulence. Discrete Fourier transform is performed on the spatiotemporal data to calculate the power spectral density $\phi(k_x, k_z, \omega)$. To obtain the one-dimensional and two-dimensional spectra, integration is required over the remaining variables of $\phi(k_x, k_z, \omega)$. In this study, the sampling interval for all numerical simulations is set to $\Delta T^+ = 0.1$. The time series (62 800 sampling time steps) are divided into 39 segments with a 50% overlap. Spectral leakage is suppressed by multiplying each segment of the time series by a Hanning window.

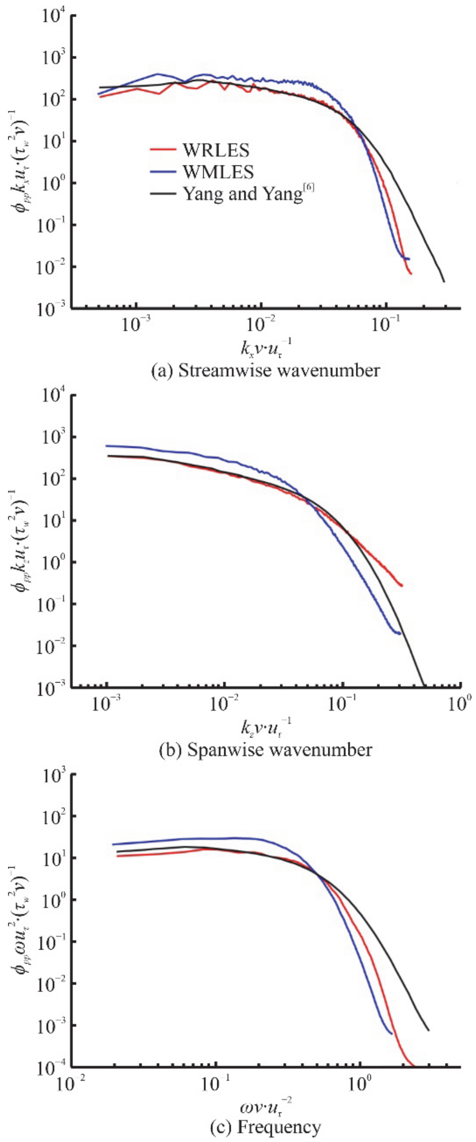


(a) Streamwise wavenumber

(b) Spanwise wavenumber

(c) Frequency

Fig. 6 One-dimensional spectra of wall pressure fluctuations

Figure 6 compares the one-dimensional spectra of wall pressure fluctuations obtained by WRLES and WMLES, including streamwise wavenumber spectrum, spanwise wavenumber spectrum, and frequency spectrum. The spectra are normalized with wall units and compared with DNS data[6]. From Figs. 6(a), 6(c), it can be observed that for both WRLES and WMLES, as the streamwise wavenumber $k_x$ and frequency $\omega$ increase, the amplitude of the one-dimensional spectra initially increases and then decreases. While the amplitude of the one-dimensional spanwise wavenumber spectrum monotonically decreases with increasing $k_z$, as shown in Fig. 6(b). This is consistent with the observations in DNS. In addition, it can be observed that the one-dimensional spectra predicted by WRLES are in excellent agreement with DNS results at low wavenumbers or low frequencies. At high wavenumbers, WRLES underestimates the spectral level in the streamwise wavenumber spectrum, while overestimating it in the spanwise wavenumber spectrum. However, for WMLES, the spectrum is slighted overpredicted in low wavenumbers ranges and underpredicted in high wavenumbers ranges.

### 3.4 *Two-dimensional spectra*

By performing a two-dimensional discrete Fourier transform on the space-time contours in Figs. 3(a), 3(c), the wavenumber-frequency spectra of velocity fluctuations can be obtained. Figure 7 shows the two-dimensional spectra of streamwise velocity fluctuations at $y^+ = 15$, normalized by $\delta$, $u_\tau$ and $\tau_w$. The three black contour lines from inside to outside correspond to −4, −5, −6. The three purple contour lines are the DNS results[6]. Since the $k_x$ - $\omega$ spectrum is centrally symmetric, we only show the part where $\omega \geq 0$. The $k_x$ - $k_z$ spectrum is symmetric about the $k_x = 0$, and we only display the part where $k_x > 0$. From Figs. 7(a), 7(c), it can be observed that the spectral energy of velocity fluctuations at any frequency is concentrated near the convection wavenumber $k_c = -\omega / u_c$, where $u_c$ is the convection velocity, approximately 60%-80% of the bulk velocity $U_\mathrm{b}$. The region where the spectral power is concentrated is called the "convective ridge". The slope of the convective ridge reflects the average convection velocity of quasi-ordered structures in turbulence. Its significance lies in the fact that when turbulent structures pass through an object at a speed equal to the convective velocity, their spatial morphology remains unchanged, consistent with the viewpoint of Taylor frozen-flow hypothesis[1]. Differing from the Taylor frozen-flow hypothesis, the width of the convective ridge region increases with increasing frequency and wavenumber, a phenomenon commonly referred to as Doppler broadening. The spectral width reflects the distortion of eddies. In practical flow scenarios, due to the random sweeping effects of large-scale eddies on small-scale eddies and the interaction among small-scale eddies, the small- scale eddies are more prone to distortion. This is manifested by a continuous increasing of spectral width with increasing frequency and wavenumber. In addition, the highest spectral level (the most energy-containing

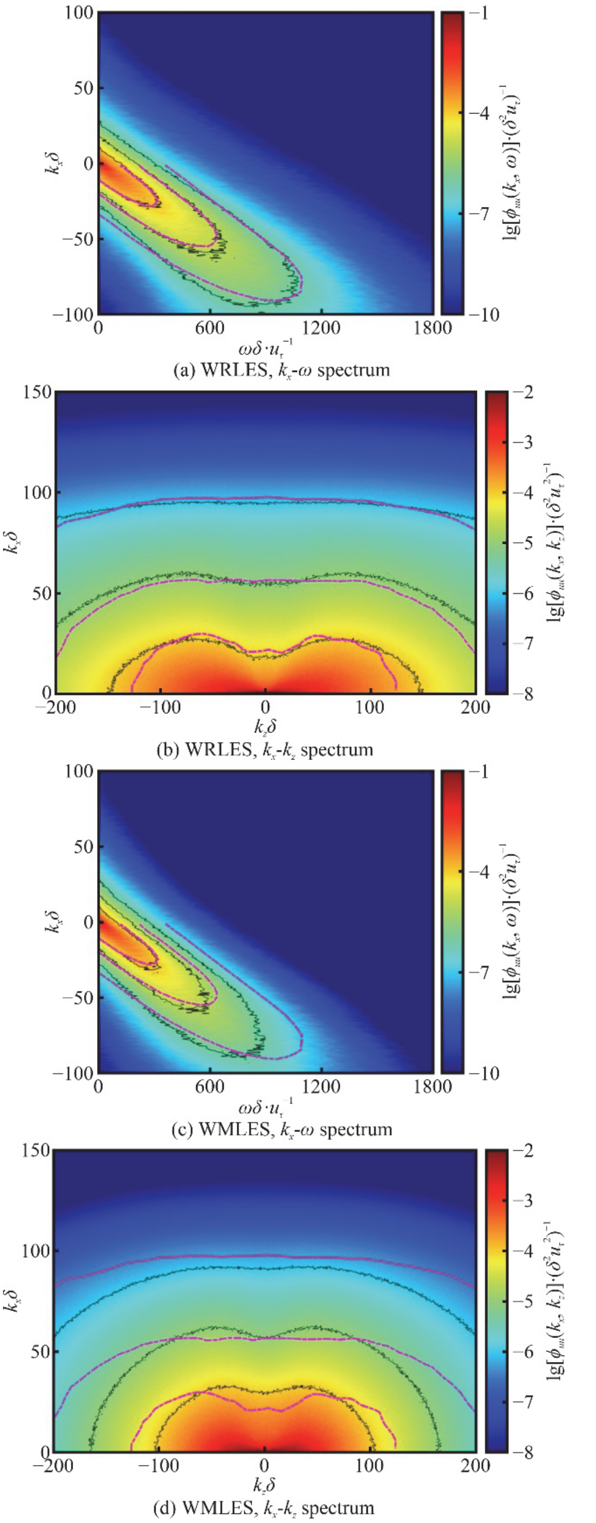


Fig. 7 Two-dimensional spectra of streamwise velocity fluctuations at $y^+ = 15$

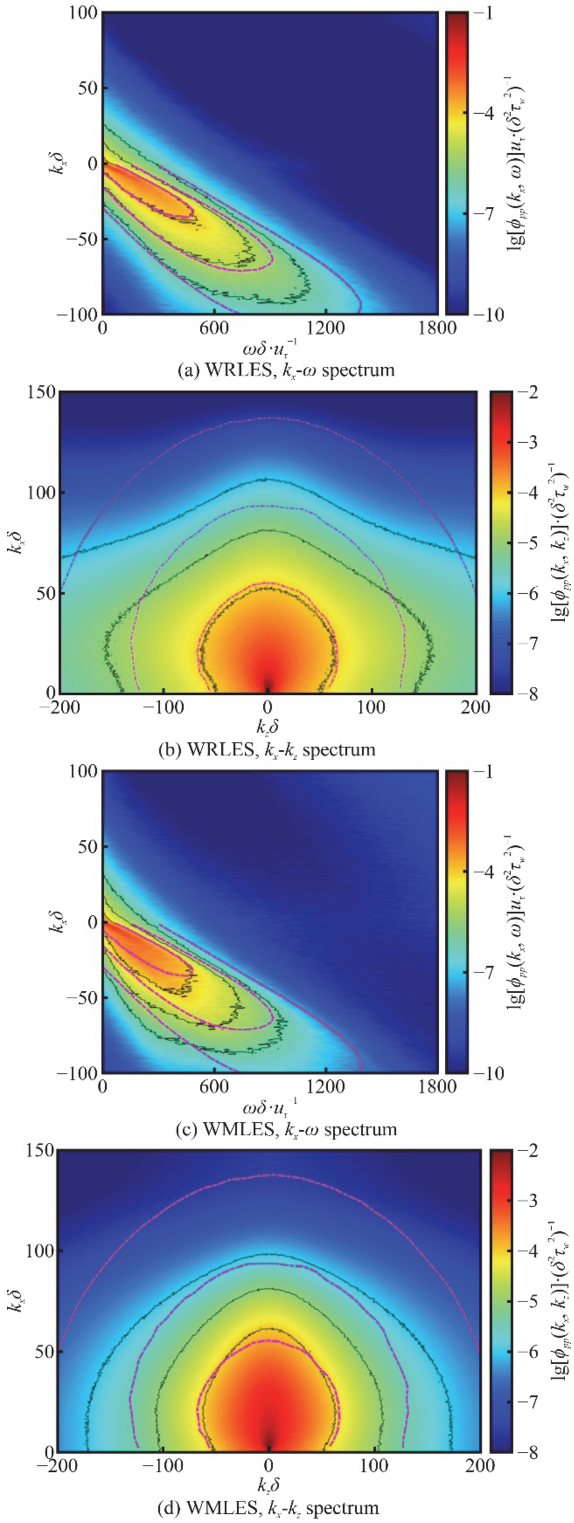


Fig. 8 Two-dimensional spectra of wall pressure fluctuations

eddies) is distributed in the low-frequency and low-wavenumber range, and the energy decreases continuously with increasing frequency and wavenumber. This is in good agreement with experiment, DNS[6] and LES[34], indicating that both methods effectively capture the essential features of space-time correlations of velocity fluctuations.

From Figs. 7(a), 7(c), it can be observed that the three contour lines of WRLES agree well with DNS results. In the case of WMLES, the innermost contour line agrees well with DNS. However, for $(\lg[\phi_{uu}(k_x,$

$\omega)]/\delta^2 u_\tau = -5, -6)$, the slope of the convection line deviates from both DNS and WRLES, indicating a slightly lower convection velocity. This may be attributed to the slight overestimation of $u_\tau$ by the current WMLES computation, resulting in a slightly lower convection velocity of near-wall small- scale vortices compared with DNS. This discrepancy is also evident in the velocity profile showed in Fig. 4, where the WMLES results are slightly lower than DNS results. In terms of $k_x$ - $k_z$ spectra, both WRLES and WMLES simulations accurately reproduced the shape of contours. The contours from WRLES agree well with DNS, with only a slight overestimation of energy distribution in the spanwise direction. While WMLES underestimated energy in the spanwise direction, with contours contracting more rapidly.

Figure 8 shows the two-dimensional spectra of wall pressure fluctuations. Compared with the $k_x$ - $\omega$ spectra of velocity fluctuations, the $k_x$ - $\omega$ spectra of wall pressure fluctuations still exhibit energy concentration in the form of convective ridges, as shown in Figs. 8(a), 8(c). The Doppler shift and Doppler broadening phenomena are also well manifested in the $k_x$ - $\omega$ spectra of wall pressure fluctuations, indicating that the space-time correlation of wall pressure fluctuations is primarily contributed by the mean flow velocity and random sweeping effects. As the $k_x$ approaches zero, the contours gradually contract towards $(k_x, \omega) = (0, 0)$, especially at innermost contour line. Meanwhile, in Figs. 8(b), 8(d), the contour lines of the $k_x$ - $k_z$ spectra also exhibit a phenomenon of contraction, which is different from that of velocity fluctuations. Previous study[6] has attributed this phenomenon to the rapid source term in the pressure Poisson equation. The contraction behavior indicates that as $k_x$ increases from zero, the spectra first increase and then decrease within a small range, consistent with the characteristics observed in the one-dimensional spectra shown in Figs. 6(a), 6(c).

For WRLES, whether in the $k_x$ - $\omega$ spectrum or the $k_x$ - $k_z$ spectrum, the contour lines of the wall pressure fluctuations in the innermost layer are in good agreement with DNS results. This indicates that WRLES can accurately predict the low-frequency wall pressure fluctuations, corresponding to large-scale flow structures in the flow field. For Fig. 8(a), as $\omega$ and $k_x$ increase, the decay of wall pressure fluctuation energy is more rapid and the contour lines of WRLES contract more quickly compared with DNS results, indicating that high-frequency wall pressure fluctuations are not well resolved. Due to the modelling for subgrid scale eddies, the underestimation of high-frequency components is not surprising. But it also indicates that predicting wall pressure fluctuations may require finer grids compared with near-wall velocity fluctuations. For Fig. 8(b), the shapes of the two contour lines at high frequency $(\lg[\phi_{pp}(k_x, k_z)]/\delta^2\tau_w^2 = -5, -6)$ do not resemble the semicircular shape presented in DNS. The $k_x$ - $k_z$ spectrum from WRLES exhibits rapid energy decay in the streamwise direction but slower decay in the spanwise direction, which is similar to the characteristics presented in the one-dimensional spectra in Figs. 6(a), 6(b). Considering that the WALE model used in this study is an isotropic SGS model, while near-wall turbulence exhibits strong anisotropy. Meanwhile, the first-layer cell of present WRLES exhibits poor isotropy, with a relatively large size difference between the streamwise and wall-normal directions. The isotropy of the first-layer cell in WMLES is relatively better, and the shape of the contour lines is also closer to DNS, as shown in Fig. 8(d). All of these factors indicate that isotropic SGS models may struggle to accurately predict the spatial distribution of wall pressure fluctuations using the anisotropy meshes.

Similar to the phenomenon observed in the wavenumber-frequency spectra of velocity fluctuations, another worth noting point is the divergence in the slope of the convection line in the $k_x$ - $\omega$ spectrum of wall pressure fluctuations between WMLES and DNS. Figure 9 show the wavenumber-dependent convection velocities of wall pressure fluctuation. The convection velocity is defined as:

$$u_c(k_x) = -\frac{\omega_c(k_x)}{k_x} \tag{7}$$

$$\left[\frac{\partial \phi_{pp}(k_x, \omega)}{\partial \omega}\right]_{\omega=\omega_c(k_x)} = 0 \tag{8}$$

For wavenumber-dependent convection velocity shown in Fig. 9, the convection velocity decreases continuously with increasing streamwise wavenumber. This suggests that due to the constraints imposed by the wall, the convection velocity of small-scale eddies is lower than that of large-scale eddies. Among them, the results of WRLES agree well with DNS, while the convection velocity of WMLES is lower than that of DNS, especially in the wavenumber range of $-k_x\delta > 20$. The discrepancy might stem from an overestimation of the wall shear stress by the current WMLES, consequently leading to deviations in the convection line slope and contour line of wavenumber-frequency spectra compared with DNS.

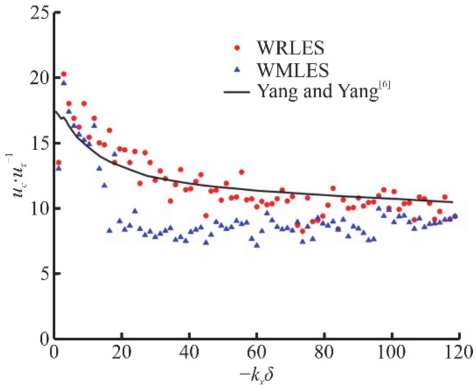

Fig. 9 Convection velocity of wall pressure fluctuation as a function of wavenumber

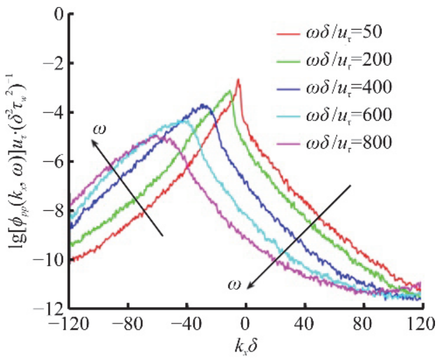

(a) WRLES

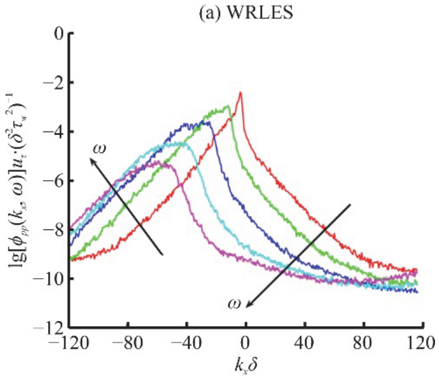

(b) WMLES

Fig. 10 Wavenumber-dependent spectra of wall pressure fluctuations at various frequencies

To further quantitatively compare the $k_x$ - $\omega$ spectra of wall pressure fluctuation, Fig. 10 shows the wavenumber spectra of wall pressure fluctuations at various frequencies. Both WRLES and WMLES effectively captured the fundamental characteristics of the $k_x$ - $\omega$ spectra of wall pressure fluctuations. As the frequency increases, the spectra level in the viscous region gradually increases, while the level in the low wavenumber region decreases. In addition, as the frequency increases, the width of the convection region expands and the spectra level decreases. At the low frequency, the wavenumber spectrum is roughly symmetrical about the convective ridge. In the high-frequency region, the spectra level of the convection region predicted by WMLES is significantly lower than that of WRLES. This discrepancy may be attributed to the relatively coarse near-wall mesh of WMLES, which does not capture the small-scale vortex structures in the high-frequency region effectively. Besides, it is worth noting that the WMLES result exhibits a certain level of background energy away from the convective ridge, indicated by higher spectral levels in the $|k_x\delta| > 80$ region. This suggests that the pressure field might be aliased, potentially contaminating the one-dimensional spectra of wall pressure fluctuations.

## 4. Conclusions

In this paper, turbulent channel flow at $Re_\tau \approx 1\,000$ is numerically simulated using both WRLES and WMLES methods to investigate their capability in predicting the space-time correlations of near-wall velocity and pressure fluctuations. Various spectral analysis techniques are employed to provide a more comprehensive understanding of the WMLES. The main conclusions drawn from this study are as follows:

In terms of mean flow quantities, the introduction of the wall model allows LES to predict the near-wall mean velocity profile accurately even on relatively coarse near-wall grids. With grid points placed at the peak of the near-wall Reynolds stress in the present WMLES setup, both WRLES and WMLES accurately predict the Reynolds stress components. Besides, WRLES and WMLES effectively capture the multiscale characteristics of near-wall turbulence and reproduce the velocity streak structures that are closely associated with the generation and self-sustenance of near-wall turbulence.

In terms of the space-time correlations of near-wall turbulent fluctuations, the result shows that both WRLES and WMLES can effectively capture the fundamental characteristics of the turbulence space-time correlations. Doppler shifts due to the convection velocity and Doppler broadening caused by the random sweeping effects of large-scale eddies are observed in the wavenumber-frequency spectra. Meanwhile, the space-time correlations of wall pressure fluctuations exhibit similar characteristics with the velocity fluctuations at $y^+ = 15$ and the convection velocity of wall pressure fluctuations is very close to that of velocity fluctuations at $y^+ = 15$. However, both WMLES and WRLES show a faster contraction of the contours in the wavenumber-frequency spectra of wall pressure fluctuations at high frequencies and wavenumbers compared with DNS. In contrast, their predictions for the wavenumber-frequency spectra of velocity fluctuation are more consistent with DNS. For the convection velocity of wall pressure fluctuations, WRLES shows good agreement with DNS. However, due to a slight overestimation of the $u_\tau$ in WMLES, the convection velocity is underestimated in the range of $-k_x\delta > 20$. This leads to a minor deviation in the slope of the convection line in the wavenumber-frequency spectra predicted by WMLES.

Another noteworthy point in this study is that in the two-dimensional spatial spectra, WRLES slightly underestimates the spectral levels in high $k_x$ region, while slightly overestimating those in high $k_z$ region. Given the disparity in streamwise and spanwise grid sizes, the isotropic SGS models may struggle to accurately predict the anisotropy of near-wall small-scale vortices.

## Conflict of interest

All authors declare that there are no other competing interests.

## References


[1] Taylor G. I. The spectrum of turbulence [J]. *Proceedings of the Royal Society of London. Series A-Mathematical and Physical Sciences*, 1938, 164: 476-490.

[2] Kraichnan R. H. Kolmogorov's hypotheses and Eulerian turbulence theory [J]. *Physics of Fluids*, 1964, 7(11): 1723-1734.

[3] Tennekes H. Eulerian and Lagrangian time microscales in isotropic turbulence [J]. *Journal of Fluid Mechanics*, 1975, 67(3): 561-567.

[4] Lee M., Moser R. D. Direct numerical simulation of turbulent channel flow up to $Re_\tau = 5\,200$ [J]. *Journal of Fluid Mechanics*, 2015, 774: 395-415.

[5] Panton R. L., Lee M., Moser R. D. Correlation of pressure fluctuations in turbulent wall layers [J]. *Physical Review Fluids*, 2017, 2(9): 094604.

[6] Yang B., Yang Z. On the wavenumber-frequency spectrum of the wall pressure fluctuations in turbulent channel flow [J]. *Journal of Fluid Mechanics*, 2022, 937: A39.

[7] He G., Wang M., Lele S. K. On the computation of space-time correlations by large-eddy simulation [J]. *Physics of Fluids*, 2004, 16(11): 3859-3867.

[8] Wilczek M., Stevens R. J. A. M., Meneveau C. Spatio-temporal spectra in the logarithmic layer of wall turbulence: large-eddy simulations and simple models [J]. *Journal of Fluid Mechanics*, 2015, 769: R1.

[9] Piomelli U. Wall-layer models for large-eddy simulations [J]. *Progress in Aerospace Sciences*, 2008, 44(6): 437-446.

[10] Larsson J., Kawai S., Bodart J. et al. Large eddy simulation with modeled wall-stress: recent progress and future directions [J]. *Mechanical Engineering Reviews*, 2016, 3(1): 15-00418.

[11] Bose S. T., Park G. I. Wall-modeled large-eddy simulation for complex turbulent flows [J]. *Annual Review of Fluid Mechanics*, 2018, 50: 535-561.

[12] Mukha T., Rezaeiravesh S., Liefvendahl M. A library for wall-modelled large-eddy simulation based on OpenFOAM technology [J]. *Computer Physics Communications*, 2019, 239: 204-224.

[13] Zhao W., Zhou F., Fan G. et al. Assessment of subgrid-scale models in wall-modeled large-eddy simulations of turbulent channel flows [J]. *Journal of Hydrodynamics*, 2023, 35(3): 407-416.

[14] Fan G., Zhu J., Zhao W. et al. A comparative study between wall-resolved and wall-modeled large eddy simulation of turbulent channel flows [C]. *34th International Ocean and Polar Engineering Conference*, Rhodes, Greece, 2024, 220-226.

[15] Fan G., Zhao W., Wan D. Near-wall turbulent fluctuations and coherent structures in wall-modeled large-eddy simulation [J]. *Physics of Fluids*, 2025, 37(9): 95108.

[16] Iyer P. S., Malik M. R. Wall-modeled large eddy simulation of flow over a wall-mounted hump [C]. *46th AIAA Fluid Dynamics Conference*, Washington DC, USA, 2016.

[17] Ren X., Su H., Yu H. et al. Wall-modeled large eddy simulation and detached eddy simulation of wall-mounted separated flow via OpenFOAM [J]. *Aerospace*, 2022, 9(12): 759.

[18] Fan G., Liu Y., Zhao W. et al. Effect of wall stress models and subgrid-scale models for flow past a cylinder at Reynolds number 3 900 [J]. *Physics of Fluids*, 2024, 36(1): 015152.

[19] Chen S., Yang L., Zhao W. et al. Wall-modeled large eddy simulation for the flows around an axisymmetric body of revolution [J]. *Journal of Hydrodynamics*, 2023, 35(2): 199-209.

[20] He K., Zhou F., Zhao W. et al. Numerical analysis of turbulent fluctuations around an axisymmetric body of revolution based on wall-modeled large eddy simulations [J]. *Journal of Hydrodynamics*, 2024, 35(6): 1041-1051.

[21] Suga K., Sakamoto T., Kuwata Y. Algebraic non-equilibrium wall-stress modeling for large eddy simulation based on analytical integration of the thin boundary-layer equation [J]. *Physics of Fluids*, 2019, 31(7): 075109.

[22] Rezaeiravesh S., Mukha T., Liefvendahl M. Systematic study of accuracy of wall-modeled large eddy simulation using uncertainty quantification techniques [J]. *Computers and Fluids*, 2019, 185: 34-58.

[23] Yang X., Sadique J., Mittal R. et al. Integral wall model for large eddy simulations of wall-bounded turbulent flows [J]. *Physics of Fluids*, 2015, 27(2): 025112.

[24] Gao W., Zhang W., Cheng W. et al. Wall-modelled large-eddy simulation of turbulent flow past airfoils [J]. *Journal of Fluid Mechanics*, 2019, 873: 174-210.

[25] Hu X., Hayat I., Park G. I. Wall-modelled large-eddy simulation of three-dimensional turbulent boundary layer in a bent square duct [J]. *Journal of Fluid Mechanics*, 2023, 960: A29.

[26] Park G. I., Moin P. Space-time characteristics of wall-pressure and wall shear-stress fluctuations in wall-modeled large eddy simulation [J]. *Physical Review Fluids*, 2016, 1(2): 024404.

[27] Maeyama H., Kawai S. Near-wall numerical coherent structures and turbulence generation in wall-modelled large-eddy simulation [J]. *Journal of Fluid Mechanics*, 2023, 969: A29.

[28] Nicoud F., Ducros F. Subgrid-scale stress modelling based

on the square of the velocity gradient tensor [J]. *Flow, Turbulence and Combustion*, 1999, 62: 183-200.

[29] Wang M., Moin P. Dynamic wall modeling for large-eddy simulation of complex turbulent flows [J]. *Physics of Fluids*, 2002, 14(7): 2043-2051.

[30] Kawai S., Larsson J. Wall-modeling in large eddy simulation: Length scales, grid resolution, and accuracy [J]. *Physics of Fluids*, 2012, 24(1): 015105.

[31] Yang X., Park G. I., Moin P. Log-layer mismatch and modeling of the fluctuating wall stress in wall-modeled large-eddy simulations [J]. *Physical Review Fluids*, 2017, 2(10): 104601.

[32] Weller H. Controlling the computational modes of the arbitrarily structured C grid [J]. *Monthly Weather Review*, 2012, 140(10): 3220-3234.

[33] Martínez J., Piscaglia F., Montorfano A. et al. Influence of spatial discretization schemes on accuracy of explicit LES: canonical problems to engine-like geometries [J]. *Computers and Fluids*, 2015, 117: 62-78.

[34] Fan G., Chen H., Zhao W. et al. Scaling laws and space-time characteristics of wall pressure fluctuations in an axisymmetric boundary layer with varying pressure gradient [J]. *Journal of Fluid Mechanics*, 2025, 1016: A28.